Prepared for submission to JCAP
YITP-SB-16-NN

Distinguishing Dark Matter Models Using Annual Modulation

Samuel J. Witte,[a,b] **Vera Gluscevic,**[c] **and Samuel D. McDermott**[d]

[a]University of California, Los Angeles, Department of Physics and Astronomy, Los Angeles, CA 90095
[b]Fermi National Accelerator Laboratory, Center for Particle Astrophysics, Batavia, IL 60510
[c]School of Natural Sciences, Institute for Advanced Study, Einstein Drive, Princeton NJ 08540, USA
[d]C. N. Yang Institute for Theoretical Physics, Stony Brook, NY, USA

Abstract. In the event of a putative signal in future direct dark matter experiments, properly identifying the underlying dark matter-nuclei interaction promises to be a challenging task. Dark matter models that produce interactions with a different dependence on the momentum transfer (*e.g.* the spin-independent interaction and Millicharge dark matter) produce qualitatively different nuclear recoil spectra, and thus their signatures could potentially be disentangled should a significant number of events be observed simultaneously in various target nuclei. Interactions with identical momentum dependence (*e.g.* the spin-independent and anapole interaction), however, are unlikely to be identified using information on the nuclear recoil spectrum alone. The observed degeneracy between such models may be partially broken should one of the dark matter-nuclei scattering cross sections contain a non-trivial dependence on the dark matter velocity, as this produces a qualitatively different time dependence of the scattering rate. Here, we investigate the extent to which including information on both the nuclear recoil energy and the time of observed events in the analysis of future direct detection data can be used to break model degeneracies. We show that including information on the annual modulation of the rate may significantly enhance the distinguishability of dark matter models with nearly degenerate recoil spectra, but only with exposures beyond the expectations of Generation 2 direct detection experiments. I might use the word 'different' too many times...

Contents

1 Introduction

A vast array of independent astrophysical and cosmological observations testify to the existence of a non-baryonic form of matter in the universe. This so-called dark matter (DM) is the dominant source of the gravitational potential wells that dictate the dynamics and structure of the universe. Despite experimental efforts on multiple fronts, including a direct detection program that has now been mature for several decades, efforts to elucidate potential non-gravitational interactions of DM with Standard Model particles have been unsuccessful.

As the next–generation direct detection experiments that incorporate increasingly sensitive detection technologies come online, they will start to probe the final portions of DM parameter space before encountering the so-called 'irreducible neutrino background' [1–10]. Generation 2 (G2) experiments that are currently taking data (see e.g. [2]) may well be on the cusp of important discoveries, as many interesting theories of DM predict scattering cross sections that live in these portions of parameters space. For example, heavy $SU(2)$–doublet and –triplet fermions, such as the Higgsinos and the wino of supersymmetry, are expected to have cross sections of order $\sigma_{\rm SI} \sim \mathcal{O}(\text{few} \times 10^{-48})\,\text{cm}^2$ (just about an order of magnitude below the current limits []`Sam, can you add a good citation?`, fixed by their Standard Model gauge quantum numbers alone [11–13], while a heavy $SU(2)$-singlet fermion, like the bino, is around an order of magnitude lower depending on its coannihilation partner [14]. Models with kinematically suppressed tree–level scattering may also be embedded in more complete dark sectors that have loop–level cross sections in this same range [15–18].

Because so many theories can be accommodated in the parameter space that will be imminently probed by a variety of experiments, it is timely to plan for the science opportunities

associated with the first detection of DM particles. Most notably, in case of a confirmed detection, understanding the high–energy dark sector dynamics will solely rely on examining low–energy recoils of detector elements and solving the "inverse problem" to identify the right underlying description of DM–baryon interactions from the experimental measurements. On the other hand, all the information about the dark sector interactions accessible to these measurements is contained within the coefficients of the "effective field theory of dark matter direct detection" (EFT) [19, 20]. This effective description also captures the nontrivial nuclear physics induced by some of the best–motivated UV–complete theories of DM [21, 22] through an exhaustible list of DM-nuclei interactions. It thus provides a systematic framework for classifying and describing a wide variety of DM theories, and we will utilize it in this work.

However, due to Poisson noise and degeneracies in the shape of the recoil spectra amongst different interactions, proper DM model identification presents a difficult task, particularly for a single experiment. Recent studies have shown that discriminating between interactions is possible only for strong signals (with hundreds of observed recoil events), and only when measurements on targets with sufficiently diverse nuclear physics characteristics are jointly analyzed [22]. Thus, using energy spectra to break degeneracies in the DM modeling space crucially relies on "complementary" nuclear physics characteristics of available target materials [8, 22–28], but this alone does not guarantee successful model selection [22, 25].

On the other hand, almost since the dawn of direct–detection–related DM studies, the motion of Earth relative to DM bound in the galactic halo has been predicted to provide a distinctive signature of DM through the characteristic annual modulation of the expected nuclear recoil rate [29–34]. While observables associated with the annual modulation is typically assumed to take an approximately universal form (when expressed in a particular set of variables), recent work [35, 36] has pointed out that non–standard interaction cross sections containing a non–factorizable velocity dependence could produce a modulation signal that is unique to each target element. More generally, a non–trivial velocity dependence in the cross section effectively changes the phase space integral that governs the total event rate in a given experiment, producing a non-standard modulation. Thus, it may be expected that interactions differing solely by the DM velocity dependence of their corresponding cross sections may be properly identified by exploiting information on the modulation of the rate.

Motivated by this argument, here we propose that analysis of time dependence of scattering events can help discriminate between interaction models whose recoil energy spectra are otherwise degenerate on a single target material. Using the method of [22], we evaluate the enhancement in prospects for accurate model selection when the annual modulation signal is analyzed in combination with recoil–energy measurements in the future generation direct detection experiments.

In Sec. 2 we review the calculation of the direct detection scattering rate and discuss how direct detection observables differ depending on the momentum and velocity dependence of the differential cross section. Sec. 3 summarizes the models and experiments that we consider in this paper, and introduces the statistical analysis we apply in order to determine the extent to which future direct detection experiments can properly identify the underlying DM model. Results are presented for various future generation experiments in Sec. 4. We conclude in Sec. 5.

2 Scattering in Direct Detection Experiments

2.1 Direct Detection Observables

The key measurement of most direct detection experiments is the nuclear recoil energy spectrum—the number count of nuclear recoil events per recoil energy E_R, per unit time t, per unit target mass,

$$\frac{dR}{dE_R dt}(E_R, t) = \frac{\rho_\chi}{m_T m_\chi} \int_{v_{\rm min}}^{v_{\rm esc,lab}} v f(\mathbf{v}, t) \frac{d\sigma_T}{dE_R}(E_R, v) d^3 v, \tag{2.1}$$

where ρ_χ is the local DM density; m_χ is the DM particle mass; m_T is the mass of the target nucleus T; $\mathbf{v}$ is DM velocity vector of magnitude v (in the lab frame); $f(\mathbf{v}, t)$ is the observed DM velocity distribution; $d\sigma_T/dE_R = m_T \sigma_T / 2\mu_T^2 v^2$ is the differential cross section for DM scattering off a nucleus T; and $\mu_T \equiv \frac{m_T m_\chi}{m_T + m_\chi}$ is the reduced mass of the DM particle and the target nuclide. Integration limits are the minimum velocity a DM particle requires in order to impart a nuclear recoil of energy E_R, which for elastic scattering[1] is given by $v_{\rm min} = \sqrt{m_T E_R / 2\mu_T^2}$, and the Galactic escape velocity in the lab frame, $v_{\rm esc,lab}$.

The differential rate in Eq. (2.1) is determined by the experimental setup, the DM astrophysical and particle properties, the nuclear properties of the target material, and the DM–nucleus interaction.[2] For the purposes of this study, we set the astrophysical parameters to the following values [37, 38]: $\rho_\chi = 0.3$ GeV/cm^3; $v_{\rm esc} = 533$ km/sec (in the Galactic frame), and assume that $f(\mathbf{v})$ is a Maxwellian distribution in the Galactic frame, with a rms speed of 155 km/sec and a mean speed equal to the Sun's rotational velocity around the Galactic center, $v_{\rm lag} = 220$ km/sec.

The underlying particle physics interaction determines the calculation of the recoil rate through the differential scattering cross section $d\sigma_T/dE_R$ [21, 22]. This quantity has a normalization (in units of cm^2) which is a free parameter of the model. Different interactions display different functional dependences on E_R and v, as discussed in detail in Refs. [21, 22] and summarized below in Sec. 2.2.

The total rate R of nuclear recoil events (per unit time and unit mass) is given by the integral of the differential rate within the nuclear–recoil energy window $\mathcal{E}$ of a given experiment[3], $R(t) = \int_{\mathcal{E}} \frac{dR}{dE_R dt} dE_R$. In turn, the total expected number of events $\langle N_{\rm tot} \rangle$ for a fiducial target mass $\mathcal{M}_{\rm fid}$, in experiment that started observation at a time t_1 and ended at a time t_2, is given by

$$\langle N_{\rm tot} \rangle = \mathcal{M}_{\rm fid} \int_{t_1}^{t_2} \int_{\mathcal{E}} \frac{dR}{dE_R dt}(E_R, t)\, dE_R\, dt. \tag{2.2}$$

[1] We restrict our attention for the remainder of this paper to DM-nuclei elastic scattering, and defer the subject of proper identification of scattering kinematics to later work.

[2] Throughout this paper we use T to denote the nuclear target and N to denote a nucleon, either neutron n or proton p

[3] For simplicity, we assume unit efficiency of detection within the analysis window, and rescale individual experimental exposures to take this assumption into account when choosing experimental parameters to represent the capabilities of G2 experiments.

2.2 Momentum and Velocity Dependence

Traditional focus on the two standard scattering cases, spin–independent (SI) and spin–dependent (SD) scattering (the former involves coherent contributions from the entire nucleus, resulting in a cross section that scales quadratically with nucleon number, while the latter scales with the total nuclear spin), obscures the richness of phenomenologies which can arise when these two standard interactions are suppressed [] Sam, do you have a good ref for this?. Here we summarize the effective field theory that catalogues all possible energy and velocity dependencies of the cross section, and thus delineates the modeling space for interactions probed by these experiments in most general terms. In the Sec. 3.1, we highlight several well–motivated examples of interesting scattering models which we use in this work to examine the extent to which including time information can enhance identification of the underlying DM model.

The effective field theory of DM direct detection [19, 20] relies on an expansion in two small kinematic variables: $|\vec{q}|/m_N$, where $\vec{q}$ is the change in momentum of the DM particle during the scattering, and $|\vec{v}_\perp|$ is the orthogonal component of the relative velocity of the initial–state particles. For an incoming (outgoing) DM three–momentum $\vec{p}(\vec{p}')$, incoming (outgoing) nuclear three–momentum $\vec{k}$ $(\vec{k}')$, and a reduced mass $\mu_{\chi N} \equiv m_\chi m_N/(m_\chi + m_N)$, these factors are $\vec{q} = \vec{p}' - \vec{p} = \vec{k} - \vec{k}'$, and $\vec{v}_\perp = \frac{\vec{p}}{m_\chi} - \frac{\vec{k}}{m_N} + \frac{\vec{q}}{2\mu_{\chi N}}$, respectively. The momentum transfer is directly related to the nuclear recoil energy as $\vec{q}^2 = 2m_T E_R$. We use m_T and m_N, for effectively the same thing, we can reduce this to one?

These expansion parameters are of the same order of magnitude, but it is important to note that they manifest differently in the observables of the scattering events (see *e.g.* [22] for a comprehensive discussion). In particular, terms that enter at higher order in $|\vec{q}|/m_N$ deliver a vanishing event rate at both small and large momentum transfer (or recoil–energy), with a maximum rate at some intermediate recoil energy, producing a "turnover feature" in the recoil–energy spectrum. Light mediator models can alternatively contain factors of $m_N/|\vec{q}|$, producing a steep enhancement of the recoil spectra at low values of E_R. On the other hand, higher–order terms in $|\vec{v}_\perp|$ produce rates that monotonically decrease with energy and are quantitatively similar to observables produced by the standard SI and SD interactions.

As was demonstrated by Ref. [22], interactions that feature different momentum dependence can be differentiated from each other using a single nuclear target, provided a sufficiently large number of events are observed; however, the latter class of models—those that differ only by the power of velocity dependence—are far more difficult to disentangle, leaving substantial degeneracy between well–motivated interaction models. In the following, we develop an intuition for how this degeneracy might be overcome, using annual modulation and time dependence of the scattering rate.

2.3 Time Dependence

In Eq. (2.1), the differential rate of nuclear recoils is explicitly denoted as depending on time, which arises as a consequence of the Earth's harmonic motion around the Sun. This motion causes the DM phase space observable by direct detection experiments to modulate, resulting in a time dependent scattering rate that is expected to vary with time on the order of a few percent. The expected phase and amplitude of the modulation depend strongly on the astrophysical and particle properties of

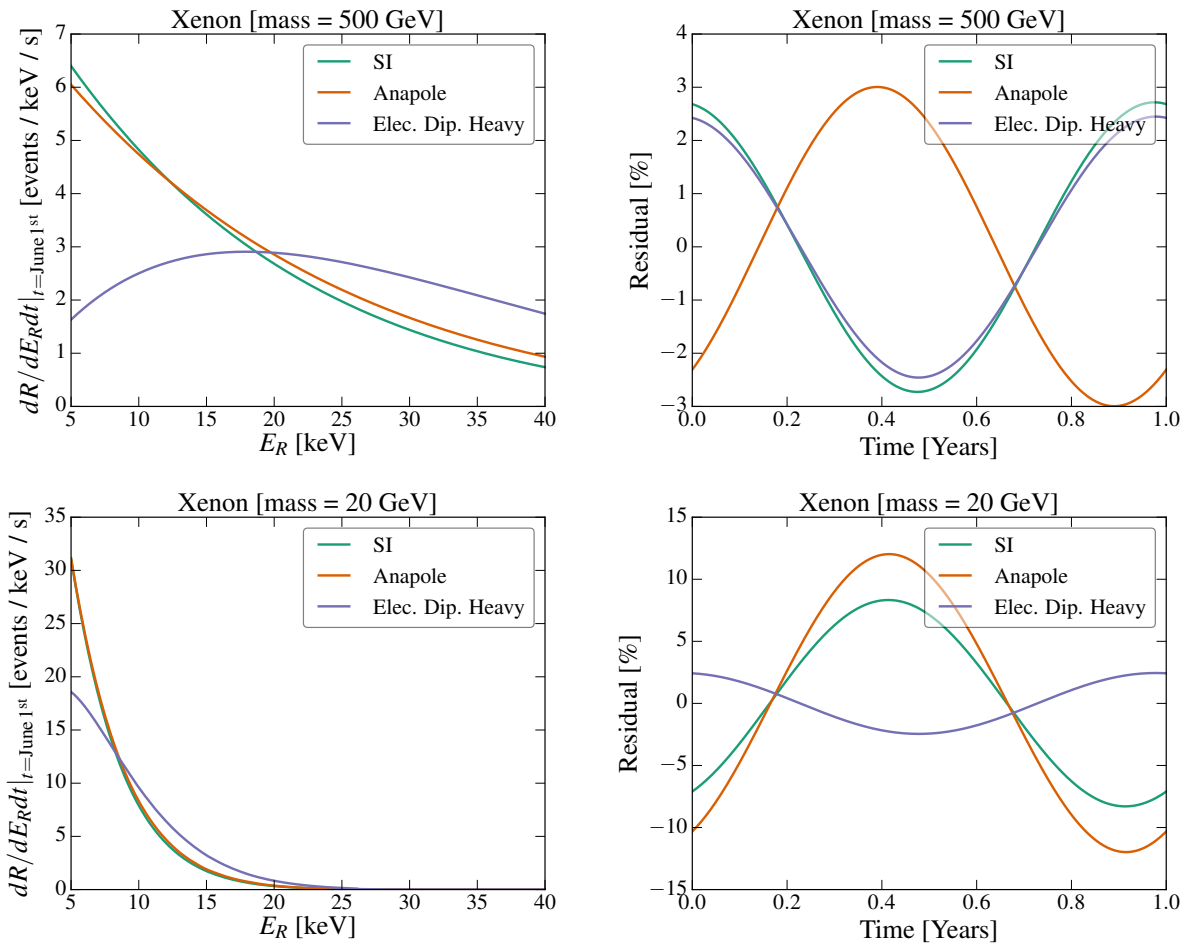

Figure 1. Comparison of the nuclear–recoil energy spectra (left column) and annual modulation signals (right column) between the SI (teal), anapole (orange), and ED-heavy (violet) interaction models on a xenon target, where the cross sections have been normalized to the current LUX 90% confidence level [43]. *Left:* Differential rate evaluated at June 1^{st} as a function recoil energy for a 500 GeV (top) and 20 GeV (bottom) DM particle. *Right:* Residual event rate (fractional deviation in the total event rate) as a function of time, for a 500 GeV (top) and 20 GeV (bottom) DM particle.

DM (see *e.g.* [33**? ?**]). For example, it was recently shown that the gravitational focusing of DM by the Sun produces a characteristic energy dependence in the phase of the modulation [33, 39–42, 44].

To illustrate the qualitative differences of the annual modulation and recoil spectrum arising from interactions with a differing functional dependence on the momentum transfer and DM velocity, we plot in Fig. 1 a comparison of the energy spectra (left column) and time dependence of the rate (right column) for several DM-nuclei interactions; specifically, we plot these observables for the standard SI (teal), anapole (orange), and heavy–mediator electric dipole (ED–heavy) (violet) interactions (see Sec. 3.1 for a more detailed definition of the models). The top (bottom) panels of Fig. 1 correspond to a 500 (20) GeV DM particle. Instead of showing the differential rate as

a function of time in the right–hand panels we show the residuals, defined as the fractional deviation from the time–averaged energy–integrated rate. Note, for example, that the energy spectra for the SI and ED–heavy interactions are distinct in a way that the SI and anapole interactions are not; thus, discerning the SI and anapole hypotheses using the energy spectrum alone is quite challenging, given even the most optimistic expectations for the Poisson noise [22].

However, the annual–modulation signatures of the SI and anapole models can be very different, owing to a non–trivial ($\sim |\vec{v}_\perp|^2$) velocity dependence of the anapole cross section. This non-trivial velocity dependence alters the velocity integral in Eq. (2.1), and consequently leads to a different time dependence of the total event rate (see Figs. 1-3 of [36] for overview of time-dependent behavior of various v-dependent cross sections). For large enough DM mass, this can produce a nearly *opposite modulation phase* between the standard SI scenario and the anapole case! Furthermore, differential cross sections which contain multiple non–negligible terms with different velocity dependences can produce annual modulation signals entirely unique to a given target element [35, 36]. The time variation of the rate, and thus the differences between the annual modulation produced by these models, is typically expected to be small – on the order of a few percent. Nonetheless, we will show in the following that this small difference in the characteristic time dependence of the rate for different models can be used to supplement the information contained in the energy spectrum and substantially aid the process of model selection on single nuclide targets employed by future experiments. In the following analysis, we incorporate the effect of gravitational focusing by the Sun following the procedure of [44].

3 Distinguishing Scattering Models

Our approach, outlined below, follows that of Ref. [22]. We being in Sec. 3.1 by identifying various realistic models which produce DM-nuclei interactions with a similar dependence on the momentum transfer but a different dependence on the DM velocity (*i.e.* models with nearly degenerate recoil spectra but qualitatively different annual modulation). Assuming a particular DM model and mass, we simulate events in future direct detection experiments assuming optimistically that the true cross section is at the current 90% confidence level. This procedure is repeated for many realizations in order to capture in the impact of Poisson noise on future data analyses (refer to Sec. 3.2 for specific details). We then perform a Bayesian model selection analysis between two models with nearly degenerate recoil spectrum but differing time dependence in order to quantitatively assess the impact that including time information may potentially have on proper model identification. The details of this statistical procedure are outline in Sec. 3.3.

3.1 Summary of Models

In this section, we illustrate a generic model which can give rise to various DM-nuclei interactions that contain non-standard dependencies on the momentum transfer and DM velocity. We emphasize that the discussion below is simply one illustration that gives rise to operators that we are interested in studying, and is by no means an exhaustive list of models which can lead to these types of interactions.

In order to assess the benefit from considering time dependence of the scattering signals in direct–detection analyses with future data, we focus on a generic extension of the Standard Model, represented by a hidden $U(1)'$ that has several charged fermions X_i and a heavy gauge boson

A'_μ with mass M that kinetically mixes with the Standard Model photon. At high energies, the Lagrangian contains

$$\mathcal{L} \supset -m_X \bar{X}_i X^i + i\bar{X}_i \not{\partial}_{ij} X^j - \frac{1}{2}M^2 A'_\mu A'^\mu - \frac{1}{4}F'_{\mu\nu}F'^{\mu\nu} - \frac{\epsilon}{2}F'_{\mu\nu}F^{\mu\nu}\,, \tag{3.1}$$

where $F_{\mu\nu}$ and $F'_{\mu\nu}$ are the field strength tensor of the photon and the heavy gauge boson, respectively (*i.e.* $F_{\mu\nu} \equiv \partial_\mu A_\nu - \partial_\mu A_\nu$). At low energies, the A'_μ and most X particles are integrated out. We assume a mass hierarchy that results in an electrically neutral fermion χ as the lightest degree of freedom in the dark sector, thereby providing a DM candidate. Because of the kinetic mixing, the state χ couples to the Standard Model nucleon current [21],

$$\mathcal{J}_\mu = \partial^\alpha F_{\alpha\mu} = e\sum_{n,p} \bar{N}\left(Q_N \frac{K_\mu}{2m_N} - \tilde{\mu}_N \frac{i\sigma_{\mu\nu}q^\nu}{2m_N}\right) N, \tag{3.2}$$

where $Q_{p(n)} = 1(0)$ are the nucleon charges in units of the electron charge e, $K_\mu/2 = (k_\mu + k'_\mu)/2$ is the average nucleon momentum, and $\tilde{\mu}_N = \frac{\text{magnetic moment}}{\text{nuclear magneton}}$ is the dimensionless magnetic moment of the nucleon.

The details of the masses and charges of the dark fermions X_i that constitute or couple to the DM χ will determine interaction that is measured in an experiment. We will use $\mathcal{O}^\mu_\chi$ to denote the Lorentz-vector fermion bilinear that couples to the current in Eq. (3.2). Because we assume χ is electromagnetically neutral, the possible $\mathcal{O}^\mu_\chi$ are [21, 22]

$$\mathcal{O}^\mu_{\chi,\text{Anapole}} = g^{\text{Anapole}}\bar{\chi}\gamma^\mu\gamma_5\chi, \tag{3.3}$$

$$\mathcal{O}^\mu_{\chi,\text{MD}} = \frac{g^{\text{MD}}}{\Lambda}\bar{\chi}i\sigma^{\mu\nu}q_\nu\chi, \tag{3.4}$$

$$\mathcal{O}^\mu_{\chi,\text{ED}} = \frac{g^{\text{ED}}}{\Lambda}\bar{\chi}i\sigma^{\mu\nu}\gamma_5 q_\nu\chi. \tag{3.5}$$

If we had alternatively taken the mass of the new gauge boson to be small relative to the characteristic scale of momentum transfer, the dipole interactions would be described by:

$$\mathcal{O}^\mu_{\chi,\text{MD}} = g^{\text{MD}}\bar{\chi}i\sigma^{\mu\nu}\chi, \tag{3.6}$$

$$\mathcal{O}^\mu_{\chi,\text{ED}} = g^{\text{ED}}\bar{\chi}i\sigma^{\mu\nu}\gamma_5\chi. \tag{3.7}$$

As stated above, the interaction operator for χ is determined by the dynamics of the X fermion(s). The anapole current in Eq. (3.6) will arise if charged $X^\pm$ states condense to form a neutral Majorana state χ [45]. The dipole currents form if an electromagnetically neutral X^0 couples to an electromagnetically charged pair of partner $X^\pm$ particles (of appropriate spin) [46]. The scale at which the charged X states are integrated out is Λ.

The simplicity of the model in Eq. (3.1) and the rich assortment of momentum and velocity dependencies that appear in the associated EFT operators illustrates the generic nature of these interactions. We list the EFT classification of these operators in Tab. 1. (This is an abbreviated version of the more exhaustive table that appeared in [22], using results of [21, 22]). In this work, we will focus on differentiating DM-nuclei interactions that have the same momentum scaling but different velocity dependence.

Model name	Lagrangian	$\vec{q}$, v Dependence
SI	$\frac{g}{M^2}\bar{\chi}\chi\bar{N}N$	1
Anapole	$\frac{g}{M^2}\bar{\chi}\gamma^\mu\gamma_5\chi\,\mathcal{J}_\mu$	$v_\perp^2, \vec{q}^2/m_N^2$
Magnetic Dipole (Heavy)	$\frac{g}{\Lambda M^2}\bar{\chi}\sigma^{\mu\nu}\chi\,q_\nu\mathcal{J}_\mu$	$\frac{\vec{q}^4}{\Lambda^4} + \frac{\vec{q}^2 v_\perp^2}{\Lambda^2}, \vec{q}^4/\Lambda^4$
Electric Dipole (Heavy)	$\frac{g}{\Lambda M^2}\bar{\chi}\sigma^{\mu\nu}\gamma_5\chi\,q_\nu\mathcal{J}_\mu$	$\vec{q}^2/\Lambda^2$
Magnetic Dipole (Light)	$\frac{g}{\Lambda}\bar{\chi}\sigma^{\mu\nu}\chi F_{\mu\nu}$	$1 + \frac{v_\perp^2 m_N^2}{\vec{q}^2}$, 1
Electric Dipole (Light)	$\frac{g}{\Lambda}\bar{\chi}\sigma^{\mu\nu}\gamma_5\chi F_{\mu\nu}$	$m_N^2/\vec{q}^2$

Table 1. Selection of operators along with their EFT dependences, adapted from [22]. The labels 'Light' and 'Heavy' in the dipole models denote the magnitude of the mediator mass relative to the characteristic momentum transfer. The nucleon electromagnetic current $\mathcal{J}_\mu$ is defined in Eq. (3.2); the transverse velocity $v_\perp$ and three–momentum transfer $\vec{q}$ are defined in terms of the collision momenta (see Sec. 2.2); and Λ is a heavy mass or compositeness scale appearing in the dipole models. Terms in the third column that induce different nuclear responses, and thus require different form factors, are separated by a comma (see *e.g.* [20] for more details).

Label	A (Z)	Energy window [keVnr]	Exposure [kg-yr]
Xe	131 (54)	5-40	2000
Ge	73 (32)	0.3-100	100
F	19 (9)	3-100	606
Xe(x3)	131 (54)	5-40	6000
Xe(x10)	131 (54)	5-40	20 000
XeG3	131 (54)	5-40	40 000

Table 2. Mock experiments considered in this work. The efficiency and the fiducialization of the target mass are included in the exposure. The first group of experiments is chosen such to be representative of the reach of G2 experiments for Xe, Ge, and F. The exposure for Xe and Ge is chosen to agree with the projected exclusion curves for LZ and SuperCDMS presented in Ref. [6]. The second group of experiments is used to quantitatively assess the impact of including the timing information as a function of the exposure, i.e. the observed number of events.

3.2 Simulations

For our simulations, we consider interactions discussed in the previous Section (summarized in Table 1), and perform our analysis for the case of a 20 GeV, 125 GeV, and 500 GeV DM particle. In all our simulations, we optimistically set the cross section to be the value maximally allowed by LUX [43] [4]. Our initial analysis focuses on G2 experiments, specifically experiments employ-

[4]We note that LUX currently produces the most constraining bounds on the models and masses of considered in this paper, although the constraint from PandaX-II is only marginally weaker [47].

Interaction /target	Xe	Ge	F
m_χ [GeV]	(20, 125, 500)	(20, 125, 500)	(20, 125, 500)
SI	(103, 99, 98)	(9, 4, 4)	(5, 1, 2)
Anapole	(103, 97, 96)	(11, 5, 5)	(36, 3, 3)
Mag. dip. heavy	(103, 89, 87)	(3, 4, 5)	(4, 1, 1)
Mag. dip. light	(103, 101, 101)	(34, 14, 14)	(86, 16, 15)
Elec. dip. heavy	(103, 91, 88)	(4, 4, 4)	(1, 0, 0)
Elec. dip. light	(103, 102, 101)	(61, 15, 14)	(40, 12, 12)

Table 3. Predicted number of events in G2 experiments for various interactions with xenon, germanium, and fluorine targets assuming a DM mass of (20 GeV, 125 GeV, and 500 GeV). The predicted numbers of events are calculated using a cross section set to the current 90% upper limits. Labels 'light' and 'heavy' denote the relative relation between the mediator mass and the characteristic scale of momentum transfer.

ing xenon, germanium, and fluorine targets. Since fluorine experiments measure only the energy integrated rate, information on recoil energies of individual events are neglected in the analysis of this experiment. The exposure and energy window of our mock experiments are summarized in Table 2. Throughout the analysis we assume unit detection efficiency and zero backgrounds. In addition to the aforementioned, we also consider the potential reach of a Generation 3 (G3) xenon experiment, as well as various xenon experiments with exposures lying somewhere between G2 and G3 (the properties of which are summarized in Table 2). The predicted number of events for each interaction considered in these mock experiments are shown in Table 3.

For each simulation, the observed number of events is obtained by randomly selecting from a Poisson distribution with a mean given by the predicted number of events calculated using Eq. (2.2). The recoil energy and time of each event is then obtained by applying a rejection sampling algorithm to the two-dimensional differential scattering rate. This procedure is repeated for $\mathcal{O}(50)$ simulations properly understand the variability of results arising from Poisson noise.

3.3 Analysis method

Within the Bayesian inference framework, the probability that the data $\vec{X}$ assigns to a given model $\mathcal{M}_j$ is given by

$$P(\mathcal{M}_j) = \frac{\mathcal{E}_j(\vec{X}|\mathcal{M}_j)}{\sum_i \mathcal{E}_i(\vec{X}|\mathcal{M}_i)}\,, \tag{3.8}$$

where $\mathcal{E}(\vec{X}|\mathcal{M})$ is the evidence of model $\mathcal{M}$, defined by

$$\mathcal{E}(\vec{X}|\mathcal{M}) = \int d\Theta\, \mathcal{L}(\vec{X}|\Theta, \mathcal{M})\, p(\Theta, \mathcal{M})\,, \tag{3.9}$$

and is intuitively understood to be the factor required to normalize the posterior $\mathcal{P}$, *i.e.*

$$\mathcal{P}(\Theta|\vec{X},\mathcal{M}) = \frac{\mathcal{L}(\vec{X}|\Theta,\mathcal{M})\,p(\Theta,\mathcal{M})}{\mathcal{E}(\vec{X}|\mathcal{M})}\,. \tag{3.10}$$

Here, $\mathcal{L}(\vec{X}|\Theta,\mathcal{M})$ is the likelihood, *i.e.* the probability of obtaining the data, given a particular model $\mathcal{M}$ and parameters Θ (for the purpose of this analysis $\Theta = \{m_\chi, \sigma_p\}$), and $p(\Theta,\mathcal{M})$ is the prior. In order to remain as agnostic as possible, we take wide priors in both m_χ and σ_p[5]. In our analysis we use an unbinned extended likelihood function of the form

$$\mathcal{L}(\vec{X}|\Theta,\mathcal{M}) = \frac{\mu^N}{N!}\,e^{-\mu}\prod_{x_i\in\vec{X}}\frac{1}{\mu}\,\frac{dR}{dE_R dt}\bigg|_{E_R,t\,=\,x_i}\,, \tag{3.11}$$

where μ is the predicted number of events, N is the number of observed events, and the product runs over all the normalized differential rate evaluated at the E_R and t values of each observed event $x_i \equiv \{E_{R,i}\,,\,t_i\}$. When time or E_R information is neglected, the differential rate is implicitly understood to be averaged over that variable.

In summary, we being our analysis by simulating data for an experiment (or experiments) assuming a particular DM model, mass, and cross section (see Sec. 3.2). We then use PyMultiNest to reconstruct the posterior defined in Eq. (3.10), and subsequently calculate the evidence for various DM models [48, 49][6]. Once the evidence of various models has been computed, one can estimate the probability of successfully being able to identify the true model using Eq. (3.8). This procedure is then repeated for $\mathcal{O}(50)$ simulations to assess the variability in successful model identification arising from Poisson fluctuations. A model is said to be correctly identified if the probability determined using Eq. (3.8) is large. For the purpose of this paper, we define the boundary for successful model identification at $P \geq 90\%$. The primary quantity of interest for future direct detection experiments is then the fraction of simulations which lead to a successful model identification.

Instead of plotting the individual probabilities of each simulation, we apply kernel density estimation (KDE) with a Gaussian kernel to determine the distribution functions of these probabilities. For of the results listed in the following section, we plot the KDE distribution for each experimental combination both with and without time, and determine the fractional success rate by integrating the distribution above the 90% threshold.

4 Results

We first examine the extent to which including time information in the analysis of G2 experiments can help break degeneracy between models with the same velocity dependence, using a study case of the SI and anapole interactions. Specifically, we simulate future data for the SI and anapole interactions and fit each simulation with these two models. We then use the Bayesian evidence generated by analyzing the fit of the two models and compute the probability of properly identifying the true underlying model (used to create a given simulation ensemble), as described in Sec. 3.3.

[5] Log priors are taken for both m_χ and σ_p, spanning $1 - 3000$ GeV in mass and 7 orders of magnitude in cross section.

[6] Multinest runs are performed with 2000 live points, an evidence tolerance of 0.1, and a sampling efficiency of 0.3.

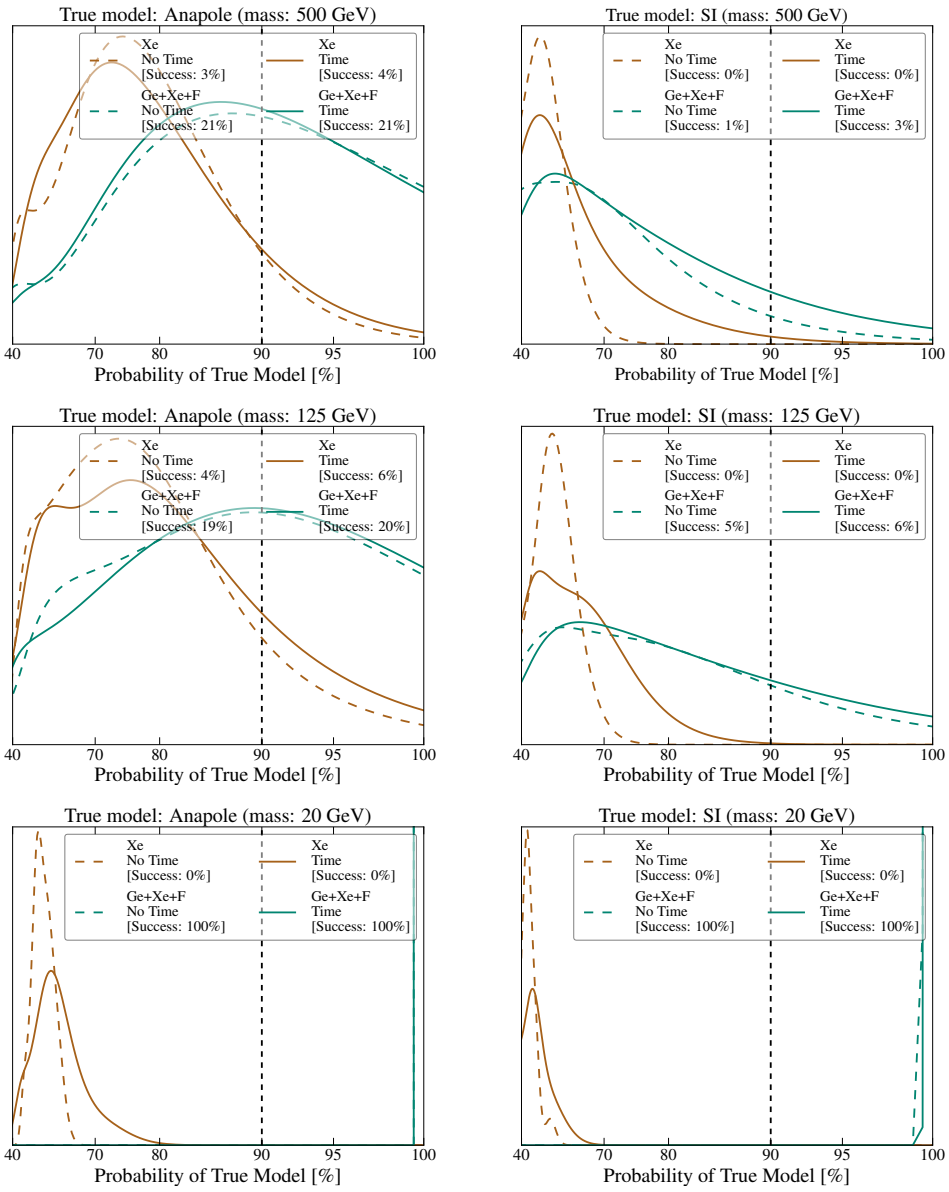

Figure 2. Model selection prospects with complimentary G2 targets. The reconstructed probability distribution functions for the probability of correctly identifying the true underlying interaction are shown for the anapole (left column) and SI (right column) interactions, for a 500 GeV (top row), 125 GeV (middle row), and 20 GeV (bottom row) DM particle mass. Cross sections are set to current upper limits, and the PDFs are all normalized to unity between 0 and 100%. Results are shown for likelihood analyses of simulated data from a xenon experiment (brown), and for a combined likelihood analyses of xenon, germanium, and fluorine experiments (teal). Solid (dashed) lines are obtained including (neglecting) time information of the recoil events. Success rate is defined to be the fraction of simulations for which the correct model was assigned $\geq 90\%$ probability.

We then derive the probability distribution function (PDF) of identifying the true underlying model from the 50 simulations that used the same input model and parameters.[7] Fig. 2 shows the results of this exercise for the anapole (left column) and SI (right column) interactions, analyzing data observed in a xenon-target experiment alone (brown) and in conjunction with a germanium- and fluorine-target experiments (teal). DM particle masses used in the simulations are: 500 GeV (top panels), 125 GeV (middle panels), and 20 GeV (bottom panels), with cross sections set to their respective current upper limits. We show the results obtained both neglecting (dashed) and including (solid) time information of the nuclear recoils.

Consistent with the results of [22], we find that the two models can be confidently distinguished for a signal close to the current detection threshold, provided G2–level exposure on xenon and a detection with a fluorine experiment, but only if data from these experiments are jointly analyzed (xenon and germanium experiments are not complementary in the sense that a joint analysis does not significantly improve prospects for model selection, and thus we do not display results for this case). For a low–mass DM particle (20 GeV), the improvement upon combining these two types of experiments is drastic: the PDF of possible model–selection outcomes entirely shifts to a delta–function at 100% probability in favor of the right model. For intermediate and high masses, the prospects are still visibly improved, but not very optimistic (at best on the level of $\sim$20% success rate), mostly due to the reduced scattering rate on fluorine.

Comparison of no-time and with-time analyses, displayed in dashed and solid lines respectively, demonstrates that inclusion of time information only negligibly changes model–selection prospects for G2 level of exposures. Given that G2 experiments will optimistically detect on the order of $\simeq 100$ events, the statistical sample will be insufficient to clearly detect differences in the modulation signal that would otherwise aid differentiation between the two interactions. It is thus not surprising that analyzing G2 data with time has a minimal effect on model selection (see *e.g.* Sec. 4 of [33] for an estimation of the number of events needed for phase measurement).

The question than arises of how many events are needed before the inclusion of time information can significantly help model selection prospects. We address this question in Figs. 3–5 for a xenon-target experiment [8]. In these figures, we show the prospects (PDF of possible analysis outcomes) of successful model selection, given different exposures in the same experiment: a 2 (brown), 6 (tan), 20 (light teal), and 40 (teal) ton–year. Simulations used for these figures all assume the anapole interaction (the results for the SI interaction are qualitatively similar and we defer the SI analogues of these figures to Appendix A), and a DM mass of 20, 125, and 500 GeV, respectively. Results are shown for analyses that neglect (dashed) and include (solid) the time dependence of the rate.

From these figures, we see that the addition of time information drastically improves prospects for successful model selection in the case of light DM particle (the solid–line PDFs are substantially shifted to the right in Fig. 3). In spite of this, a G3 xenon experiment has only a $\simeq 16\%$ chance of disentangling these two interactions. Fig. 1 gives an intuition for interpreting this outcome: both

[7] Note that, since we only consider two competing models, a PDF peaked at around 50% means that the data is most likely to be agnostic between the two models, *i.e.* they produce comparable fits. This is the most pessimistic outcome possible. A tail of the distribution at high probabilities, or a PDF shift in that direction, signifies improved model identification.

[8] We choose to illustrate this for xenon experiments as they are projected to observe far more events for the interactions considered than their germanium and fluorine based counterparts.

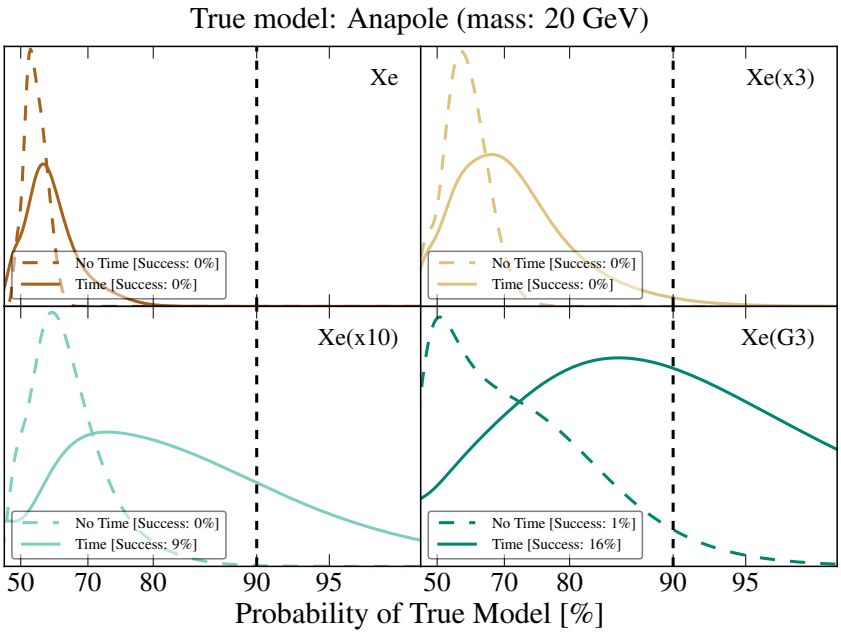

Figure 3. Model selection prospects for a single target (xenon), including (solid lines) and neglecting (dashed lines) time information in the likelihood analysis. The normalized probability distribution functions are plotted for the probability of identifying the underlying model– here, taken to be 20 GeV anapole DM. Panels from left to right, top to bottom, correspond to experimental exposures of 2 (brown), 6 (tan), 20 (light teal), and 40 (teal) ton–years, respectively. Simulations used to obtain these results all optimistically assume cross sections are at their current upper limit. Percent chance for successful model identification (defined here as having $\geq 90\%$ probability assigned to the anapole model) is provided in the legend.

the recoil spectra and the phase of the modulation of the SI and anapole interactions (measured in a xenon-target experiment) are more degenerate for light DM particles; thus, even when including time information in the analysis, a single target experiment still must observe a large even of events in order to successfully distinguish between these models.

At larger DM particle masses, however, the recoil energy spectra are less degenerate, allowing for better model discrimination at fixed exposure. This is, in part, because of a $\simeq 5$ month difference in phase between the modulation produce by the SI and anapole interactions (see again Fig. 1). Figs. 4 and 5 indeed confirm that heavier DM candidates allow for better model discrimination of these models, particularly when time is included in the analysis. From these figures, we see that including time in the analysis can improve model selection in G3 experiments by as much as $\simeq 30\%$ for heavy DM, where the phases of the modulation signal for these two interactions may be misaligned by as much as $\simeq 5$ months. Finally, it is important to keep in mind that all the results displayed in these figures assume the most optimistic number of observed recoil events. Thus, despite the improvement in model selection obtained through the inclusion of time information, it is likely that model selection with G3 experiments will still be challenging using a single target; most likely, the experiments will need to exploit target complimentarily and perform joint likelihood analyses in order to fully break the degeneracy observed between these types of models and ensure

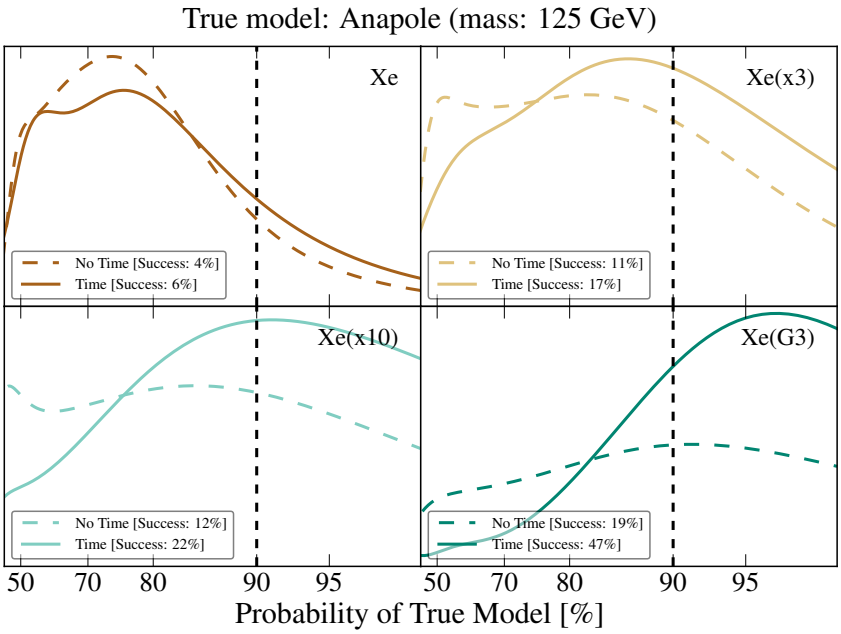

Figure 4. Same as Fig. 3 but for 125 GeV DM.

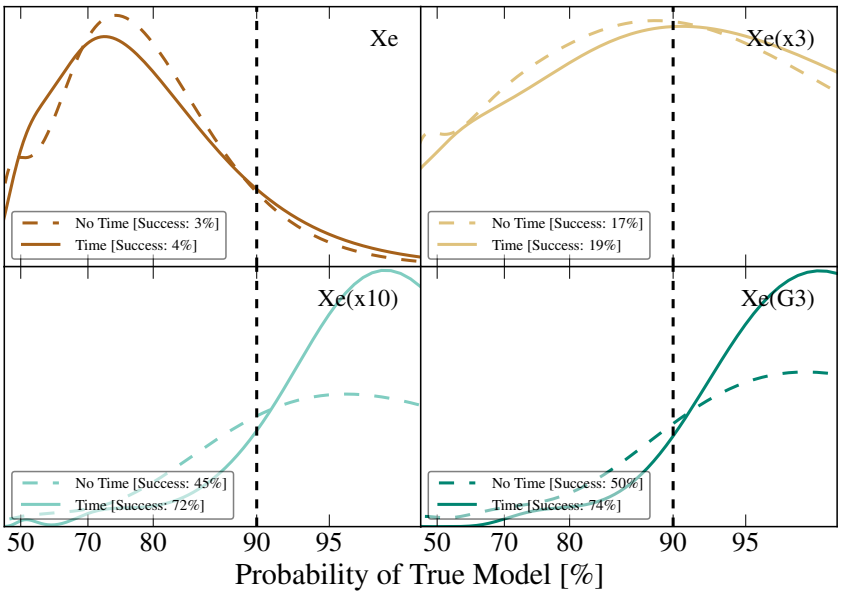

Figure 5. Same as Fig. 3 but for 500 GeV DM.

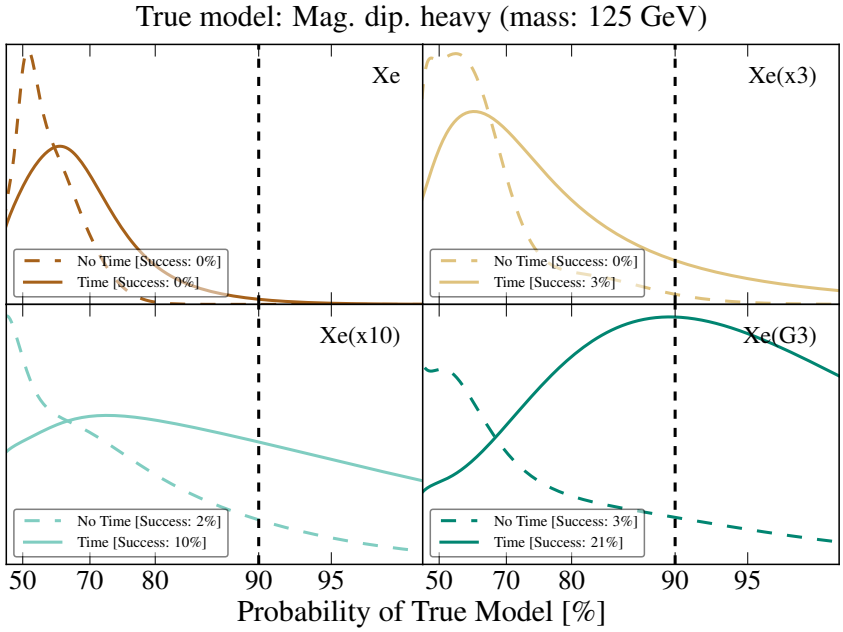

Figure 6. Same as Fig. 3, but now assessing the ability of xenon experiments to break the degeneracy of the magnetic dipole (heavy mediator) and electric dipole (heavy mediator) interactions, instead of SI and anapole interactions. Simulations assume a 125 GeV DM particle and and a magnetic–dipole interaction.

the highest chance of correctly identifying the interaction at hand.

The goal of this work was primarily a quantitative assessment of whether time information can be exploited in future direct–detection analyses to break degeneracies in the recoil spectra of different interaction models—and SI and anapole interactions provided a particularly illuminating study case for this purpose. However, the main conclusions presented in this Section hold for other sets of interaction models as well, and we now briefly illustrate this point. In Figs. 6 and 7 we consider a comparison of the magnetic dipole and electric dipole interactions for a 125 GeV DM particle, assuming a heavy (Fig. 6) and light (Fig. 7) mediator. As before, we consider putative detections in future xenon experiments with exposures varying from 2 to 40 ton–years. The results are rather similar to the SI and anapole comparison in that G3 experiments can expect a $\simeq 20\%$ improvement in model selection when time is included in the analysis, but again necessitate target complementarity to have a high chance of confidently differentiating these interactions.

5 Summary and Discussion

We have considered here the potential impact of using time information in the likelihood analysis of data from future direct detection experiments in order to break degeneracies between the recoil energy spectra of different DM–baryon interactions. Specifically, we performed a statistical assessment of the prospects for successful Bayesian model selection between different interaction models, using an ensemble of simulations that account for the impact of Poisson fluctuations on possible analysis outcomes.

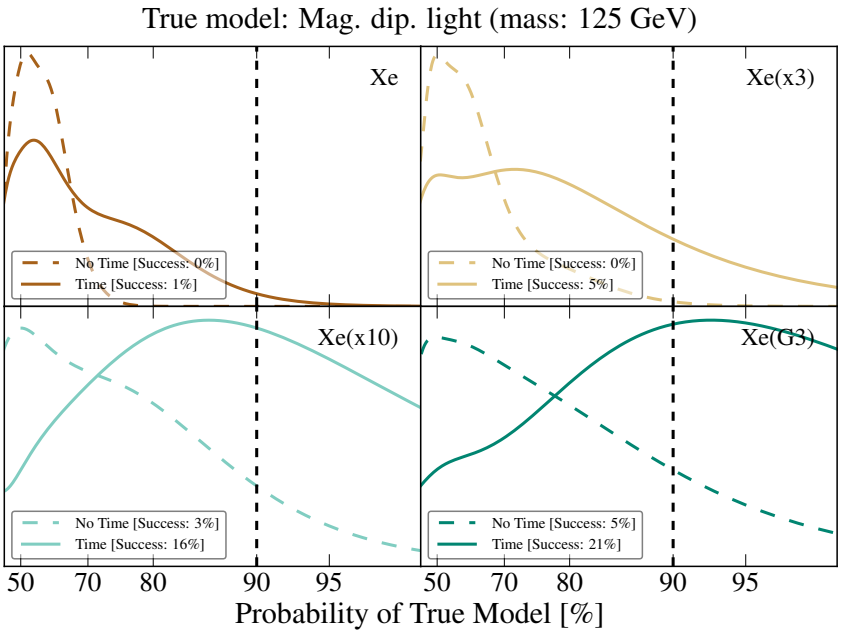

Figure 7. Same as Fig. 6 but for a light mediator case.

As a case study, we compared the standard spin–independent interaction and anapole DM, but also demonstrated that the main findings hold for other degenerate interaction models as well. We explored three different dark–matter masses, and focused specifically on the most optimistic case where the cross sections for all interactions saturate current upper limits.

We found that even under the most optimistic of circumstances, including time information in the analysis of G2 direct detection does not significantly improve prospects for distinguishing between models with degenerate recoil spectrum. Rather, correct model identification in G2 experiments will almost certainly require measurements and combined analyses on multiple target elements. We found that for the inclusion of time information to significantly increase chances for successful model selection (by $\mathcal{O}(10)\%$), given a single target element, $\mathcal{O}(1000)$ events must be observed for a 20 GeV, and $\mathcal{O}(500)$ for a 500 GeV DM particle. These numbers are consistent with the 'back-of-the-envelope' calculations performed in [33]. Furthermore, even if time information is exploited in G3 xenon experiments, target complementarity must also be exploited to unequivocally differentiate between different models. We emphasize that our analysis in maximally optimistic in the sense that our analysis uses the largest allowed cross section and completely neglecting potential backgrounds. More conservative choices would certainly reduce the ability of future experiments to properly identify the underlying interactions.

In the event of a putative signal, direct detection experiments will be charged with the difficult task of illuminating the high energy behavior of DM solely from the observed low–energy recoils. This is a particularly daunting task in light of the fact that many feasible DM models produce nearly degenerate recoil spectra. Exploiting all of the information available, including the time information of nuclear recoils, will be necessary to make definitive statements regarding the true

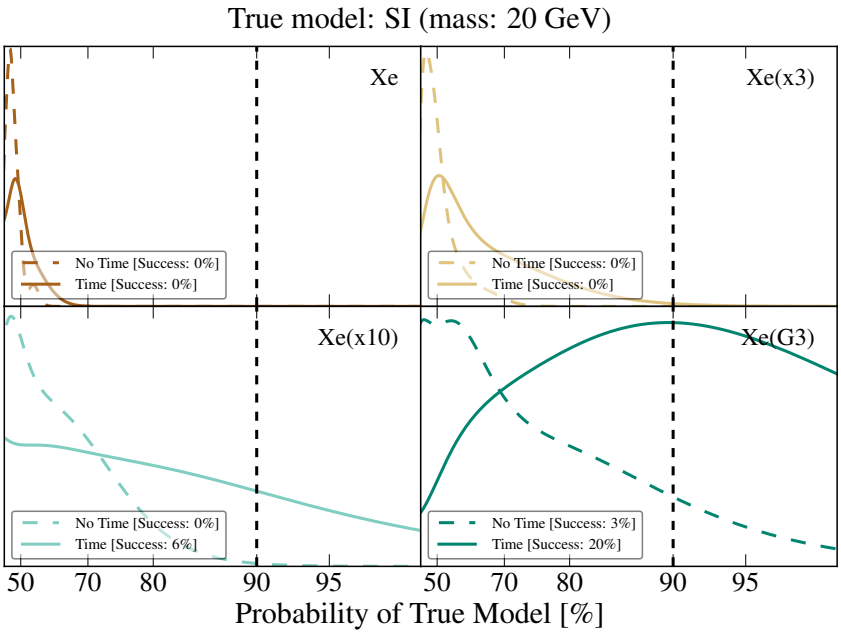

Figure 8. Same as Fig. 3 but for the SI interaction as the true model.

particle nature of DM.

Acknowledgments. SW is supported under the University Research Association (URA) Visiting Scholars Award Program, and by a UCLA Dissertation Year Fellowship. VG gratefully acknowledges the support of the Schmidt Fellowship at the Institute of Advanced Study.

A Model Selection Prospects in Xenon (SI Interaction)

We present in Figs. 8–10 the model selection prospects for various exposures on a xenon experiment, including (solid lines) and neglecting (dashed lines) information on the modulation of the recoil rate, and assuming the SI interaction is the true model. Results are shown for 20 GeV (Fig. 8), 125 GeV (Fig. 9), and 500 GeV (Fig. 10) DM particle. Results are similar to those presented in Sec. 4 for the case of the anapole interaction.

References

[1] Snowmass 2013 Cosmic Frontier Working Groups 14 collaboration, D. Bauer et al., *Dark Matter in the Coming Decade: Complementary Paths to Discovery and Beyond*, *Phys. Dark Univ.* **7-8** (2015) 16–23, [1305.1605].

[2] XENON collaboration, E. Aprile et al., *Physics reach of the XENON1T dark matter experiment*, *JCAP* **1604** (2016) 027, [1512.07501].

[3] SuperCDMS collaboration, R. Agnese et al., *Projected Sensitivity of the SuperCDMS SNOLAB experiment*, *Submitted to: Phys. Rev. D* (2016) , [1610.00006].

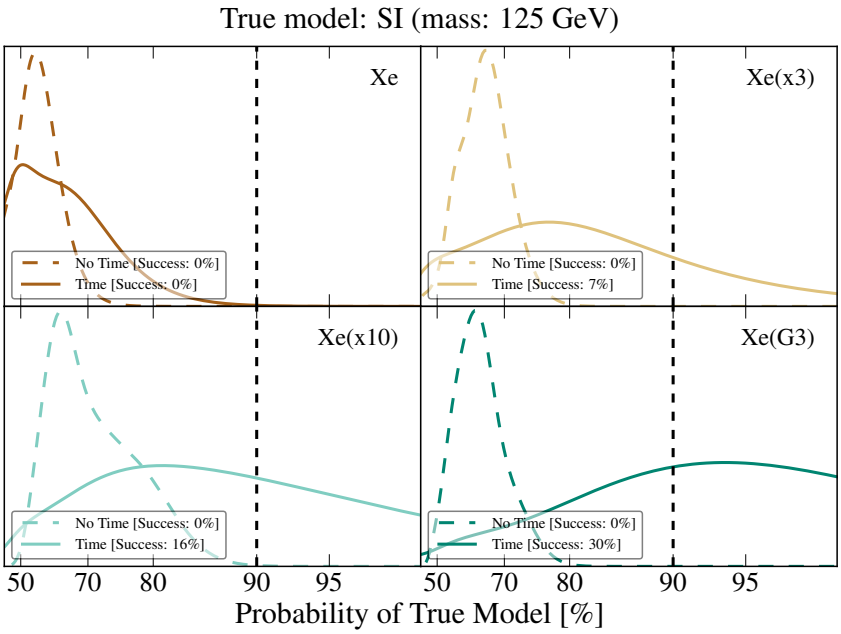

Figure 9. Same as Fig. 3 but for a 125 GeV DM and the SI interaction as the true model.

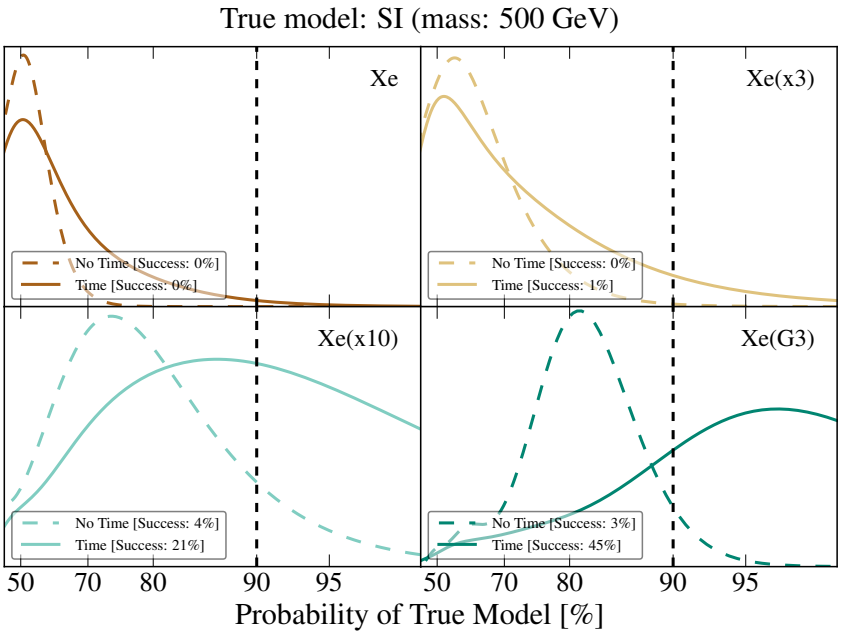

Figure 10. Same as Fig. 3 but for a 500 GeV DM and the SI interaction as the true model.

[4] D. C. Malling et al., *After LUX: The LZ Program*, 1110.0103.

[5] J. L. Newstead, T. D. Jacques, L. M. Krauss, J. B. Dent and F. Ferrer, *Scientific reach of multiton-scale dark matter direct detection experiments*, *Phys. Rev.* **D88** (2013) 076011, [1306.3244].

[6] P. Cushman et al., *Working Group Report: WIMP Dark Matter Direct Detection*, in *Proceedings, 2013 Community Summer Study on the Future of U.S. Particle Physics: Snowmass on the Mississippi (CSS2013): Minneapolis, MN, USA, July 29-August 6, 2013*, 2013. 1310.8327.

[7] J. Billard, L. Strigari and E. Figueroa-Feliciano, *Implication of neutrino backgrounds on the reach of next generation dark matter direct detection experiments*, *Phys. Rev.* **D89** (2014) 023524, [1307.5458].

[8] F. Ruppin, J. Billard, E. Figueroa-Feliciano and L. Strigari, *Complementarity of dark matter detectors in light of the neutrino background*, *Phys. Rev.* **D90** (2014) 083510, [1408.3581].

[9] J. H. Davis, *Dark Matter vs. Neutrinos: The effect of astrophysical uncertainties and timing information on the neutrino floor*, *JCAP* **1503** (2015) 012, [1412.1475].

[10] J. B. Dent, B. Dutta, J. L. Newstead and L. E. Strigari, *Effective field theory treatment of the neutrino background in direct dark matter detection experiments*, *Phys. Rev.* **D93** (2016) 075018, [1602.05300].

[11] R. J. Hill and M. P. Solon, *Universal behavior in the scattering of heavy, weakly interacting dark matter on nuclear targets*, *Phys. Lett.* **B707** (2012) 539–545, [1111.0016].

[12] R. J. Hill and M. P. Solon, *WIMP-nucleon scattering with heavy WIMP effective theory*, *Phys. Rev. Lett.* **112** (2014) 211602, [1309.4092].

[13] R. J. Hill and M. P. Solon, *Standard Model anatomy of WIMP dark matter direct detection II: QCD analysis and hadronic matrix elements*, *Phys. Rev.* **D91** (2015) 043505, [1409.8290].

[14] A. Berlin, D. S. Robertson, M. P. Solon and K. M. Zurek, *The Bino Variations: Effective Field Theory Methods for Dark Matter Direct Detection*, 1511.05964.

[15] S. Ipek, D. McKeen and A. E. Nelson, *A Renormalizable Model for the Galactic Center Gamma Ray Excess from Dark Matter Annihilation*, *Phys. Rev.* **D90** (2014) 055021, [1404.3716].

[16] S. D. McDermott, *Lining up the Galactic Center Gamma-Ray Excess*, *Phys. Dark Univ.* **7-8** (2014) 12–15, [1406.6408].

[17] T. Appelquist et al., *Stealth Dark Matter: Dark scalar baryons through the Higgs portal*, *Phys. Rev.* **D92** (2015) 075030, [1503.04203].

[18] T. Appelquist et al., *Detecting Stealth Dark Matter Directly through Electromagnetic Polarizability*, *Phys. Rev. Lett.* **115** (2015) 171803, [1503.04205].

[19] A. L. Fitzpatrick, W. Haxton, E. Katz, N. Lubbers and Y. Xu, *The Effective Field Theory of Dark Matter Direct Detection*, *JCAP* **1302** (2013) 004, [1203.3542].

[20] N. Anand, A. L. Fitzpatrick and W. C. Haxton, *Weakly interacting massive particle-nucleus elastic scattering response*, *Phys. Rev.* **C89** (2014) 065501, [1308.6288].

[21] M. I. Gresham and K. M. Zurek, *Effect of nuclear response functions in dark matter direct detection*, *Phys. Rev.* **D89** (2014) 123521, [1401.3739].

[22] V. Gluscevic, M. I. Gresham, S. D. McDermott, A. H. G. Peter and K. M. Zurek, *Identifying the Theory of Dark Matter with Direct Detection*, *JCAP* **1512** (2015) 057, [1506.04454].

[23] S. D. McDermott, H.-B. Yu and K. M. Zurek, *The Dark Matter Inverse Problem: Extracting Particle Physics from Scattering Events*, *Phys. Rev.* **D85** (2012) 123507, [1110.4281].

[24] A. H. G. Peter, V. Gluscevic, A. M. Green, B. J. Kavanagh and S. K. Lee, *WIMP physics with ensembles of direct-detection experiments*, *Phys. Dark Univ.* **5-6** (2014) 45–74, [1310.7039].

[25] V. Gluscevic and A. H. G. Peter, *Understanding WIMP-baryon interactions with direct detection: A Roadmap*, *JCAP* **1409** (2014) 040, [1406.7008].

[26] R. Catena, *Prospects for direct detection of dark matter in an effective theory approach*, *JCAP* **1407** (2014) 055, [1406.0524].

[27] R. Catena, *Analysis of the theoretical bias in dark matter direct detection*, *JCAP* **1409** (2014) 049, [1407.0127].

[28] J. B. Dent, L. M. Krauss, J. L. Newstead and S. Sabharwal, *General analysis of direct dark matter detection: From microphysics to observational signatures*, *Phys. Rev.* **D92** (2015) 063515, [1505.03117].

[29] K. Freese, J. A. Frieman and A. Gould, *Signal Modulation in Cold Dark Matter Detection*, *Phys. Rev.* **D37** (1988) 3388–3405.

[30] K. Freese, M. Lisanti and C. Savage, *Colloquium: Annual modulation of dark matter*, *Rev. Mod. Phys.* **85** (2013) 1561–1581, [1209.3339].

[31] S. K. Lee, M. Lisanti and B. R. Safdi, *Dark-Matter Harmonics Beyond Annual Modulation*, *JCAP* **1311** (2013) 033, [1307.5323].

[32] V. Britto and J. Meyers, *Monthly Modulation in Dark Matter Direct-Detection Experiments*, *JCAP* **1511** (2015) 006, [1409.2858].

[33] E. Del Nobile, G. B. Gelmini and S. J. Witte, *Gravitational Focusing and Substructure Effects on the Rate Modulation in Direct Dark Matter Searches*, *JCAP* **1508** (2015) 041, [1505.07538].

[34] C. Kouvaris and N. G. Nielsen, *Daily modulation and gravitational focusing in direct dark matter search experiments*, *Phys. Rev.* **D92** (2015) 075016, [1505.02615].

[35] E. Del Nobile, G. B. Gelmini and S. J. Witte, *Target dependence of the annual modulation in direct dark matter searches*, *Phys. Rev.* **D91** (2015) 121302, [1504.06772].

[36] E. Del Nobile, G. B. Gelmini and S. J. Witte, *Prospects for detection of target-dependent annual modulation in direct dark matter searches*, *JCAP* **1602** (2016) 009, [1512.03961].

[37] J. Bovy and H.-W. Rix, *A Direct Dynamical Measurement of the Milky Way's Disk Surface Density Profile, Disk Scale Length, and Dark Matter Profile at 4 kpc $\lesssim R \lesssim$ 9 kpc*, *Astrophys. J.* **779** (2013) 115, [1309.0809].

[38] T. Piffl et al., *The RAVE survey: the Galactic escape speed and the mass of the Milky Way*, *Astron. Astrophys.* **562** (2014) A91, [1309.4293].

[39] J. M. A. Danby and G. L. Camm, *Statistical dynamics and accretion*, *Monthly Notices of the Royal Astronomical Society* **117** (1957) 50–71, [http://mnras.oxfordjournals.org/content/117/1/50.full.pdf+html].

[40] K. Griest, *Effect of the Sun's Gravity on the Distribution and Detection of Dark Matter Near the Earth*, *Phys. Rev.* **D37** (1988) 2703.

[41] P. Sikivie and S. Wick, *Solar wakes of dark matter flows*, *Phys. Rev.* **D66** (2002) 023504, [astro-ph/0203448].

[42] M. S. Alenazi and P. Gondolo, *Phase-space distribution of unbound dark matter near the Sun*, *Phys. Rev.* **D74** (2006) 083518, [astro-ph/0608390].

[43] D. S. Akerib et al., *Results from a search for dark matter in the complete LUX exposure*, 1608.07648.

[44] S. K. Lee, M. Lisanti, A. H. G. Peter and B. R. Safdi, *Effect of Gravitational Focusing on Annual Modulation in Dark-Matter Direct-Detection Experiments*, *Phys. Rev. Lett.* **112** (2014) 011301, [1308.1953].

[45] J. Bagnasco, M. Dine and S. D. Thomas, *Detecting technibaryon dark matter*, *Phys. Lett.* **B320** (1994) 99–104, [hep-ph/9310290].

[46] N. Weiner and I. Yavin, *UV completions of magnetic inelastic and Rayleigh dark matter for the Fermi Line(s)*, *Phys. Rev.* **D87** (2013) 023523, [1209.1093].

[47] PandaX-II collaboration, A. Tan et al., *Dark Matter Results from First 98.7 Days of Data from the PandaX-II Experiment*, *Phys. Rev. Lett.* **117** (2016) 121303, [1607.07400].

[48] Buchner, J., Georgakakis, A., Nandra, K., Hsu, L., Rangel, C., Brightman, M. et al., *X-ray spectral modelling of the agn obscuring region in the cdfs: Bayesian model selection and catalogue*, *A&A* **564** (2014) A125.

[49] F. Feroz, M. P. Hobson and M. Bridges, *MultiNest: an efficient and robust Bayesian inference tool for cosmology and particle physics*, *Mon. Not. Roy. Astron. Soc.* **398** (2009) 1601–1614, [0809.3437].